A&A 463, 635–640 (2007)
DOI: 10.1051/0004-6361:20066572
© ESO 2007

Astronomy & Astrophysics

IRAS 08572+3915: constraining the aromatic versus aliphatic content of interstellar HACs⋆,⋆⋆,⋆⋆⋆

E. Dartois[1], T. R. Geballe[2], T. Pino[3], A.-T. Cao[3], A. Jones[1], D. Deboffle[1], V. Guerrini[4], Ph. Bréchignac[3], and L. d'Hendecourt[1]

[1] Institut d'Astrophysique Spatiale, UMR-8617, Université Paris-Sud, bâtiment 121, 91405 Orsay Cedex, France
e-mail: emmanuel.dartois@ias.u-psud.fr
[2] Gemini Observatory, 670 North Aòhoku Place, Hilo, HI 96720, USA
[3] Laboratoire de Photophysique Moléculaire, UPR 3361, Université Paris-Sud, bâtiment 210, 91405 Orsay Cedex, France
[4] Service d'Aéronomie, UMR 7620, Route des Gatines, BP 3, 91371 Verrières Le Buisson, France

Received 16 October 2006 / Accepted 22 November 2006

ABSTRACT

We analyze dust features present in the mid-infrared (Spitzer) and recently published L-band (UKIRT) spectra of the infrared galaxy IRAS 08572+3915. The line of sight toward the AGN nucleus crosses a high column density of carbonaceous dust whose characteristic absorption features appear clearly. They provide a real insight into the chemical environment of the diffuse interstellar medium. Thanks to the moderate redshift of IRAS 08572+3915, the wavelength of the aromatic CH stretching mode is free of major telluric lines, and a strong observational constraint of $H_{sp2}/H_{sp3} \leq 0.08$ has been determined. This limit clearly shows that the bonding of hydrogen atoms in interstellar hydrogenated amorphous carbon is highly aliphatic. The presence of a broad absorption feature centered at 6.2 μm, probably arising from olefinic/aromatic structures, corresponds to the backbone of this carbonaceous material, which is the major carbon-containing component of the interstellar medium along this line of sight.

Key words. ISM: abundances – ISM: dust, extinction – galaxies: individual: IRAS 08572+3915 – galaxies: ISM

1. Introduction

Dust in the diffuse interstellar medium (DISM) is observed in the infrared through its characteristic absorption and emission features. In absorption, the strongest known diffuse interstellar feature, which is also the most accessible from ground-based spectroscopy, lies at 3.4 μm. The strongest examples of this feature in the Galaxy are along lines of sight toward sources in or near the Galactic center. The 3.4 μm feature possesses substructures identified with methyl (-CH_3) and methylene (-CH_2-) group stretching modes (e.g., Duley et al. 1983). Many candidate analog materials, produced in laboratory experiments have been proposed as the carriers of this absorption band (e.g. Mennella et al. 2002; Pendleton et al. 2002; Chiar et al. 2002; Chiar et al. 1998; Geballe et al. 1997; Tielens et al. 1996; Tielens et al. 1996; Sandford et al. 1995; Ehrenfreund et al. 1991; McFadzean et al. 1989; Butchart et al. 1986; Jones et al. 1983; Moore & Donn 1982, and references in these articles). Because the aliphatic stretching mode is found in a multitude of materials, one must also rely on other evidence to constrain the identification. In particular the presence or absence of mid-infrared spectral signatures, sought after from both ground and space, has allowed the number of viable candidates to be reduced (Pendleton et al. 2002; Spoon et al. 2002; Dartois et al. 2004a).

Understanding the origin and evolution of the 3.4 μm absorption band is of uppermost importance, as its carrier contains a significant fraction of the total available cosmic carbon (5 to 30%, Duley et al. 1998; Sandford et al. 1991). Furthermore, key questions, yet to be answered, arise when comparing diffuse absorption features, which are dominated by an aliphatic component, to the aromatic emission features, the so-called "PAH" (Polycyclic Aromatic Hydrocarbon) features. It is not yet known if these materials are two ubiquitous coexisting components of the DISM and other phases of the interstellar medium, or are two different evolutionary stages of the same material, or even if one can meaningfully compare absorption strengths to emission strengths along the same line of sight to answer such questions.

Recent infrared observations show that the aliphatic 3.4 μm absorption feature is also found in some external galaxies believed to possess dusty toroids of matter enshrouding active galactic nuclei and emitting brightly in the infrared (Imanishi 2000; Spoon et al. 2002). The profiles of the feature measured toward these extragalactic sources (Wright et al. 1996; Dartois et al. 2004a; Mason et al. 2004) are similar to those in our Galaxy, suggesting that both the lengths of carbon chains and the natures of the CH stretching modes are similar. However, in most cases the low redshift and/or the strong aromatic starburst 3.3 μm emission band make it difficult to firmly constrain the contribution of absorbing aromatic material in the same diffuse interstellar matter that produces the 3.4 μm aliphatic absorption.

⋆ Based on observations made with the Spitzer Space Telescope (GO-3336 program), which is operated by the Jet Propulsion Laboratory, California Institute of Technology under NASA contract 1407.

⋆⋆ Based on data obtained at the United Kingdom Infrared Telescope, which is operated by the Joint Astronomy Center on behalf of the UK Particle Physics and Astronomy Research Council.

⋆⋆⋆ Part of this work has been financed by the french CNRS program "Physique et Chimie du Milieu Interstellaire" (PCMI-CNRS). TRG's research is supported by the Gemini Observatory, which is operated by the Association of Universities for Research in Astronomy, Inc., on behalf of the international Gemini partnership of Argentina, Australia, Brazil, Canada, Chile, the United Kingdom, and the United States of America.

Article published by EDP Sciences and available at http://www.aanda.org or http://dx.doi.org/10.1051/0004-6361:20066572

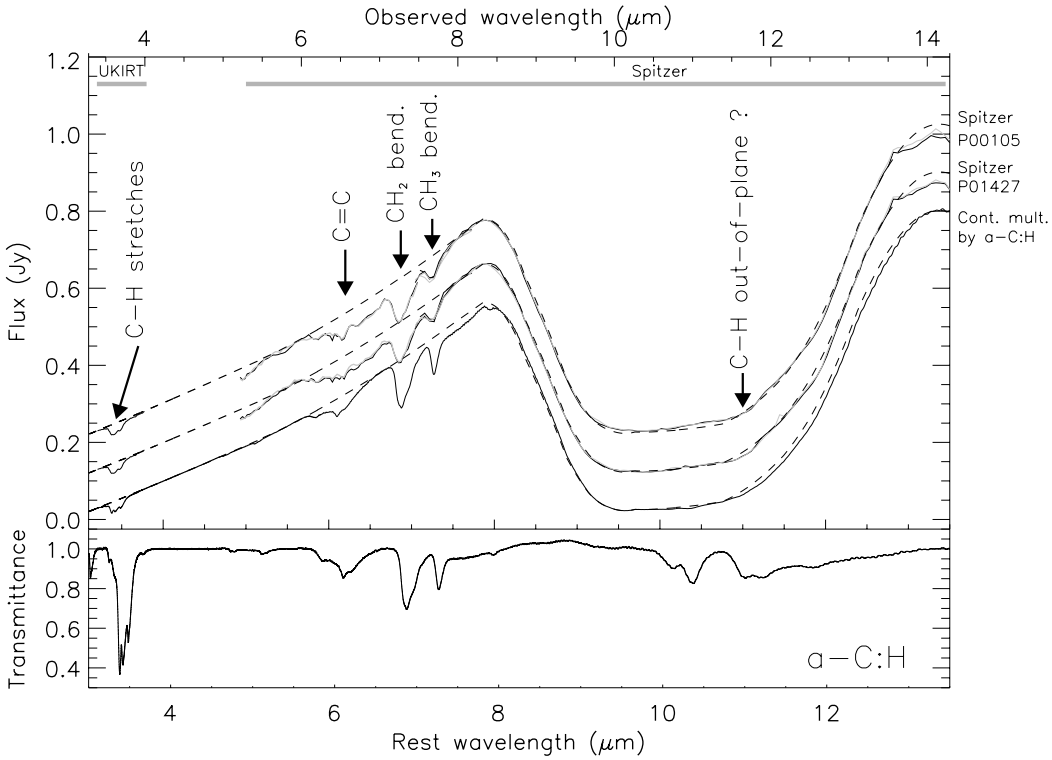

Fig. 1. Observed astronomical and laboratory spectra. The upper panel shows combined UKIRT (L band, Geballe et al. 2006) and Spitzer (programs P00105, upper curve & P01427 middle curve, offset for clarity, see also Spoon et al. 2006) spectra of IRAS 08572+3915. The observed and rest wavelength scales (adopting a redshift of $z = 0.0583$) are given at top and bottom, respectively. The estimated non-carbonacous overlying continuum is shown as dashed line. The main carbonaceous modes are indicated above the spectra. The lowest curve is the result of the multiplication of the dashed line continuum by the appropriate scaled transmittance of a laboratory a-C:H analog (Dartois et al. 2005; shown in lower panel), the resulting spectrum is shown at the bottom of the upper panel.

The aromatic absorption feature, near 3.3 μm, lies on the short wavelength side of the aliphatic absorption and, at low redshifts, is coincident with a strong telluric absorption band of CH_4, making measurement of its strength difficult.

IRAS 08572+3915 is a distant ($z = 0.0583$, Evans et al. 2002) infrared galaxy with one of the strongest known 3.4 μm absorption features (Wright et al. 1996; Imanishi et al. 2006; Mason et al. 2004). Its mid-infrared spectrum, recently observed by the Spitzer Telescope, displays the mid-infrared deformation modes of carbonaceous dust around 6.85 and 7.25 μm, which also have been found in other extragalactic sources (Spoon et al. 2006). The high H_2 column density along the line of sight toward IRAS 08572+3915 ($\sim 7 \times 10^{22}$ cm^{-2}) has enabled the first detection of the H_3^+ ion in the diffuse ISM of an external galaxy (Geballe et al. 2006). Those authors present a new medium resolution *L*-band spectrum of IRAS 08572+3915, obtained at the United Kingdom Infrared Telescope (UKIRT), that contains an accurate profile of the redshifted 3.4 μm feature and also covers the wavelength of the aromatic feature, whose wavelength is redshifted to about 3.5 μm.

Because of the moderate redshift of this galaxy and its lack of emission from aromatic species, an accurate comparison of the contributions of aromatic and aliphatic hydrocarbons along the sight to the nucleus is feasible. In this paper we use the UKIRT spectrum and recent Spitzer spectra of IRAS 08572+3915 together with laboratory spectra of dust analogues, to constrain the relative abundances of aromatic and aliphatic hydrocarbons in the DISM of this galaxy.

2. Observations

A 3.4–4.0 μm spectrum of IRAS 08572+3915 was obtained at UKIRT with its facility cooled grating spectrograph CGS4 (Mountain et al. 1990) in 1998 December. The resolving power was 1500. The spectrum is displayed on the extreme left-hand edge of Fig. 1.

Data from the programs P00105 (Spectroscopic Study of Distant ULIRGs II, P.I. James R. Houck) and P01427 (SIRTF IRS Calibration Program, P.I. Lee Armus) were retrieved from the Spitzer archive. The data consist of low-resolution spectra ($R \approx 70$–120) acquired on 2004 April 15 (P00105) and 2005 December 12 (P01427) by the Spitzer Space Telescope's Werner et al. 2004 Infrared Spectrograph (IRS) Houck et al. 2004 in the Long-Low wavelength acquisition mode, covering the 5–27 μm range. The data were reduced at the PBCD level. We focused our study on the 5.2−8.7 μm and 7.4−14.5 μm spectra, both acquired with a ramp duration of 14 seconds and 3 cycles. Small gain correction factors (less than 5%) were applied at the final data reduction step using the overlap between each sub-band to stitch the spectral segments together and produce a continuous 5.2–14.5 μm spectrum. The positive and negative spectra were treated separately in order to test the reproducibility of the features. The resultant spectra are shown in Fig. 1.

3. Results

The spectrum of IRAS 08572+3915 in Fig. 1 contains a very strong and broad absorption at 10 μm due to silicates and several less intense carbonaceous absorptions near 3.4 and 7 μm,

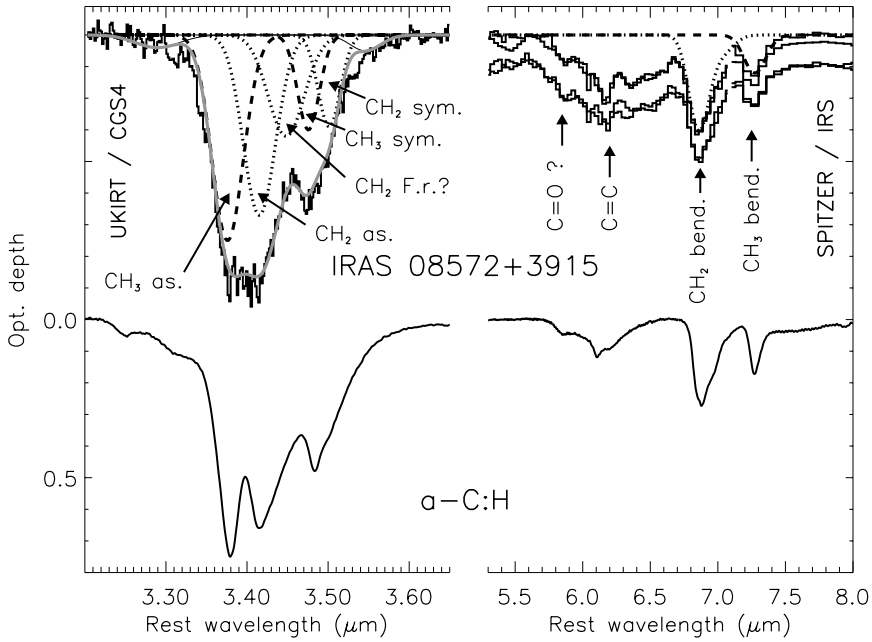

Fig. 2. *Upper panel*: optical depth spectrum of IRAS 08572+3915 based on data shown in Fig. 1. The decomposition into individual Gaussians for each vibrational mode is shown. The gray line represents the sum of these Gaussians. The Gaussian centered at 3.30 μm corresponds to the upper limit placed on the aromatic CH contribution. The 5.3–8.0 μm spectra are the individual observations from Spitzer's programs P00105 (upper trace) and P01427 (lower trace) *Lower panel*: optical depth spectrum of hydrogenated amorphous carbon, normalised to the maximum 3.4 μm optical depth in IRAS 08572+3915.

all on a rising continuum. To extract the profiles of the carbonaceous absorption features we estimated the 3.4–8.5 μm continuum by spline-fitting through a set of data points situated off of the features. This continuum is shown as dashed lines in the upper panel of Fig. 1 and the dashed lines are extended through the silicate feature. The lower panel of Fig. 1 shows the infrared spectrum of an hydrogenated amorphous carbon (HAC or a-C:H) produced at Institut d'Astrophysique Spatiale, multiplied by the non-carbonaceous continuum represented by the dashed lines, to provide the expected spectrum shown in the upper panel directly below the two observed spectra. The HAC was formed at 10 K by condensing a simple hydrocarbon precursor (hexane) and exposing the condensate to the VUV (~10 eV) photons from an H_2 discharge lamp through a MgF_2 window. The photons induce excited electronic states, creating fragments and/or radicals which recombine to form the a-C:H network at low temperature. Details are given by Dartois et al. (2005). This is an artificial way of producing astrophysical a-C:H with photon energies not exceeding the MgF_2 window cut-off (~120 nm) and at low temperature. The technique provides the highest degree of hydrogenation for such a carbonaceous network as it does not include the much more energetic ions encountered when a-C:H is produced directly in a plasma. As shown, the absorption profiles of this a-C:H are in excellent agreement with the astronomical observations *over the entire 3.2–8.0 μm wavelength range*.

To analyze the profiles of the carbonaceous features we derived the optical depth spectrum shown in Fig. 2 from the data in Fig. 1. This spectrum, shifted into the rest frame, was then fitted by four Gaussian components whose wavelengths correspond to the vibrational modes of the aromatic and aliphatic bands, and a fifth Gaussian whose central wavelength is intermediate between the symmetric and asymmetric wavelengths. The last probably is due to a Fermi resonance with the bending mode (Dartois et al. 2005), due to the proximity of the symmetric modes to the red wing of the CH_2 asymmetric mode. The central wavelengths and optical depths, widths, identifications, and integrated absorbances of all five Gaussians are given in Table 1. Note that, unlike for the *L*-band spectrum, for the 5.3–8.0 μm spectrum Gaussians are fitted only to the two narrow features at 6.85 μm and 7.27 μm; i.e., no attempt is made to fit the entire 5.3–8.0 μm spectrum. Using published values for the integrated cross-section of these modes, column densities estimates were calculated for the individual modes; these are also given in Table 1.

3.1. CH stretching modes

The contributions of the CH_2 and CH_3 stretching modes are generally estimated from the optical depths around 3.38 and 3.42 μm (e.g. Sandford et al. 1991), i.e. using only the asymmetric stretching modes. The uncertainty in the shape and contribution of the Fermi resonance makes the fitting procedure uncertain for the relatively weak symmetric modes. In Table 1 this uncertainty is reflected in the large discrepancy in derived column densities between e.g. the CH_3 asymmetric and symmetric modes. In the following we use the more secure column densities estimated from the asymmetric modes.

The important new aspect of this study with respect to previous work is the simultaneous accurate access to both the aliphatic and aromatic stretching modes. No clear absorption feature is detected at the expected position of aromatic CH stretching mode (~3.29 μm). An olefinic absorption at ~3.32 μm, present in the laboratory a-C:H, appears to produce a short wavelength wing on the asymmetric CH_3 absorption. The maximum aromatic contribution escaping detection is indicated by the shallow Gaussian centered at 3.29 μm in Fig. 2. The limit based on it implies $N(H_{arom})/N(H_{aliph}) = N(CH_{arom})/(2N(CH_2) + 3N(CH_3)) < 0.08$.

Table 1. Profile decomposition.

Wavelength[a] (μm)	mode	τ	*HWHM* (cm^{-1})	integrated absorbance[b](cm^{-1})	A(cm/group)[c] $\times10^{-18}$	column $\times10^{18}$ cm^{-2}
3.289	CH arom.	0.04	30	≤2.5	1.28[z], 1.3[y], 1.9[g], 2.0[x]	≤1.3
3.377	CH_3 as.	0.65	20	27.7	12.5[e]/12[f]	2.2/2.3
3.415	CH_2 as. + Fermi.res.	0.57&0.32	20&22	39.3	8.4[e]/7.4[f]	4.6/5.3
3.476	CH_3 sym.	0.3	13	8.3	2.0[e]/2.1[f]	4.0/4.2
3.503	CH_2 sym.	0.29	13	8.0	2.4[e]/2.1[f]	3.3/3.8
6.0–6.4	C = C stretching	–	–	≤21.6	0.1–0.25[w,x,y,z](PAHs)	≤85–220
		–	–		0.4–1.5[g](olefinic)	≤14.4–54
6.859	CH_2 def + CH_3 asym.bend.	0.3&0.05	19&19	14.2	see text	–
7.273	CH_3 sym.bend.	0.12	18	4.6	0.75[h]/0.75–1.5[g]	3.1–6.1

[a] Fitted assuming a redshift of 0.0583.
[b] Integrating optical depth under the Gaussian.
[c] Per group, i.e. per CH_2,CH_3, C = O, except CC stretching evaluated per C atom.
[e] Dartois et al. (2004a); [f] Sandford et al. (1991); [g] Wexler (1967).
[h] Estimated mean absorption per group based on the spectra of hexane at 10 K Dartois et al. (2004a).
[w] Hudgins & Sandford (1998); [x] Joblin et al. (1994); [y] Leger et al. (1989). [z] Schutte et al. (1990).

From the silicate optical depth of about 4.2 (Spoon et al. 2006), $A_V/\tau_{silicates}$ = 16.6–18.5 (Roche & Aitken 1984; Rieke & Lebofsky 1985) and $N_H/A_V = 1.9 \times 10^{21}$ cm^{-2} we obtain a total column density of elementary H of 1.3–1.5 $\times$ 10^{23} cm^{-2} as was already estimated by Geballe et al. 2006. Radiative transfer effects may weaken the silicate absorption and thus this number may be a lower limit. If it is accurate then the fraction of carbon involved in the CH stretches along this line of sight is $n(C)/n(H) = (n(CH_2)+n(CH_3))/(n(H)) = 4.5–5.8\times10^{-5}$, representing about 15% of the cosmic carbon, taking C/H = 3.7×10^{-4} as the carbon abundance.

3.2. CH bending and CC stretching modes

The bending counterparts of the CH_2 and CH_3 stretching modes are clearly seen at 6.85 μm (CH_2 deformation / CH_3 asym. bending) and 7.27 μm (CH_3 sym. bending). A column density estimate can only be obtained from the 7.27 μm feature as the 6.85 μm absorption is an unresolved blend of several modes. It can be seen that the relative abundance of the CH stretching and bending modes is in excellent agreement with the laboratory produced a-C:H analogue

The broad absorption feature in IRAS 08572+3915 extending from 6.0 to 6.4 μm is attributed to aromatic and olefinic C=C stretching modes, which are also present in the laboratory a-C:H spectra (e.g. Duley 2000; Dartois et al. 2005, and references therein). An absorption due to the carbonyl (C = O) vibration is present on the blue wing of this band near 5.8 μm; the wavelength suggests ketone (R1–C = O–R2) or aldehyde (R–C = O–H) bonding. The band may also be present as a contaminant in the laboratory spectrum in Fig. 1 and Fig. 2. Due to the high intrinsic oscillator strength of the C = O bond, it represents a very small fraction of the carbon along the line of sight. We also note that the spectrum of IRAS 08572+3915 near 3 μm shows no evidence for H_2O ice (Imanishi et al. 2006; see their Fig. 1 and Table 4.). We conservatively estimate that optical depth of the OH stretch is less than 0.2, which implies about a factor of ten lower upper limit for the optical depth of the water bending mode at 6 μm; i.e. $\tau(6.0\ \mu m) < 0.02$ (Hagen et al. (1983); D'Hendecourt & Allamandola 1986). This is well below the observed $\tau(6.2\ \mu m)$ of ≈0.15 towards IRAS 08572+3915. Thus the C=C bond must be the dominant contributor to this absorption.

The simultaneous presence of the C=C stretching mode and absence of aromatic CH underline the fact that olefinic/aromatic (i.e. sp^2 bonded) carbon forms the backbone of carbonaceous structures producing these absorption bands. Neutral (and/or very large ionized) PAHs are grossly inconsistent with observed strengths of the absorption bands in the C=C region. Indeed, using measured or computed 6.2 μm integrated cross-sections, for neutral PAHs, which range from 0.1 to 0.25×10^{-18}cm/C (e.g. Hudgins & Sandford 1998; Joblin et al. 1994; Schutte et al. 1990; Leger et al. 1989), the estimated column density of 9–22×10^{19}C/cm^2 would represent more than ≈160% of the available cosmic carbon estimated from the silicate absorption band. Olefinic compounds (transvinylene, vinyl, vinylidene, ...) have integrated absorption cross-section in the 0.4–1.5 $\times$ 10^{-18}cm/C range Wexler 1965, corresponding to no more than 30% of the available cosmic carbon if the total integrated absorbance is due to olefinic C = C stretching.

4. Discussion

The IRAS 08572+3915 object harbors an AGN whose energetic photons have been reprocessed to provide the infrared continuum against which hydrocarbons absorptions are seen. This dust probably results from the ISM of one of the two interacting galactic pair funneling near the nucleus responsible for the strong infrared emitter. The carriers of the a-C:H absorptions, unlike PAHs emitters encountered in Starburst galaxies, are probably not very small. The corresponding heat capacity being high, and if no specific mechanism can isolate the vibrations in a small subpart of the network, they are not subject to emission in the infrared following the absorption of energetic photons, but rather redistribute the energy among network modes and re-emit in the FAR-IR/mm. The observed astronomical column densities and the cosmic abundance of carbon place some constraints on the abundances of hydrocarbons along the line of sight to IRAS 08572+3915. We have shown that toward IRAS 98572+3915 about 15% of carbon atoms in the sp^3 bonding state (C_{sp^3}) are linked to hydrogen atoms, with a ratio of $CH_2/CH_3 \approx 2$. The hydrogen content is thus constrained to be $x(H)/x(C_{sp^3}) \approx 2.33$, where $x(i)$ is the fraction of atoms in the sp^3 material that are element i. If no hydrogen is bonded to the C_{sp^2}, which represents at most 85% of the total carbon, the hydrogen content of the carbonaceous material can be calculated

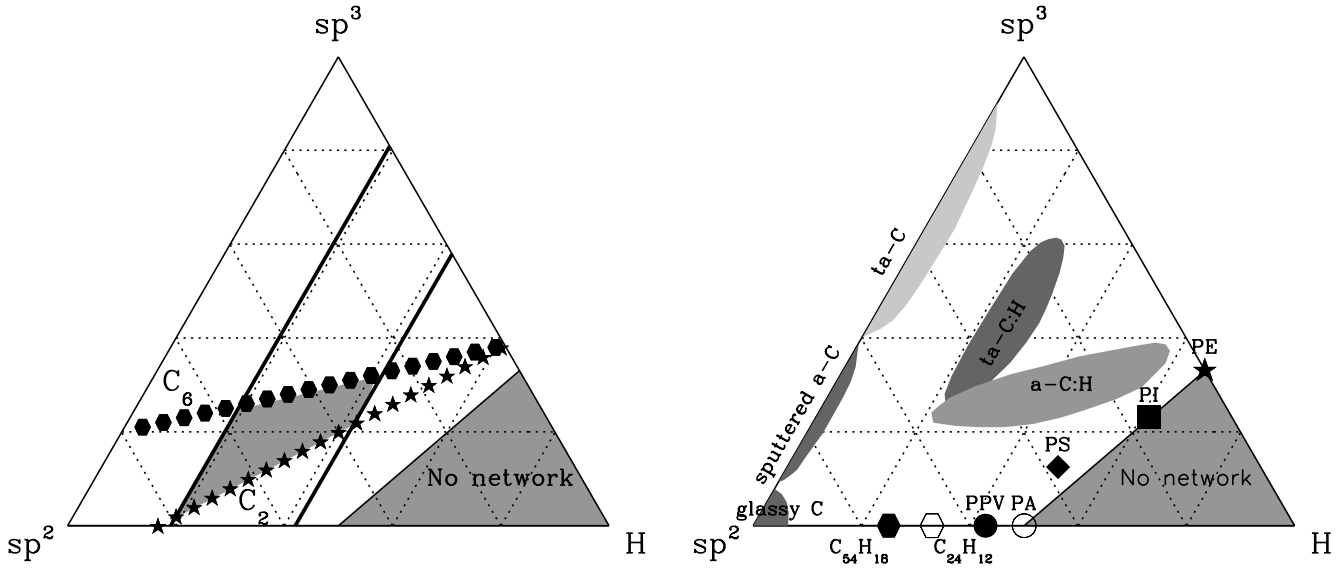

Fig. 3. Ternary phase diagrams for an amorphous carbon phase containing hydrogen (H), sp^2 and sp^3 carbon atoms. The pure sp^2 carbon pole corresponds to graphite and pure sp^3 to diamond. The filled regions around the hydrogen poles delineate where no carbonaceous network can develop. Dotted lines indicate in steps of 0.2 the fraction of each species. *Left diagram*: constraints from astronomical observations (thick lines) coupled to an RCN network comprising C_6 aromatic units (filled hexagons) or C_2 ethylenic units (filled stars). *Right diagram*: positions of the materials produced in laboratory experiments (Ferrari & Robertson 2000). Polymers lie near to and define the "no network" limit. Some common polymers – polyethylene (PE, filled star), polyisoprene (PI, filled square)), polystyrene (PS, filled diamond), polyacetylene (PA, circle), polyphenylvinylene (PPV, filled circle) – are plotted to illustrate this point. Purely aromatic molecules are defined on the sp2 to PA line (coronene and circumcoronene are plotted with hexagons). The diamond-like materials are represented with filled regions. Note the excellent overlap between the constraints from astronomical observations and the region of stability for hydrogenated amorphous carbon.

from:

$$\frac{x(C_{sp^3})}{x(C_{sp^2}) + x(C_{sp^3})} \approx 0.15 \approx \frac{x(H)}{2.33[x(C_{sp^2}) + x(C_{sp^3})]}.$$

This equation is coupled to $x(H) + x(C_{sp^2}) + x(C_{sp^3}) = 1$, because the carbonaceous material is almost entirely made of hydrogen and carbon atoms. Assuming that the percentage of cosmic carbon in C_{sp^3} material lies between 10% (if the line of sight cosmic carbon available is underestimated because of radiative transfer effects) and 30% (if either the fraction of cosmic carbon in this carbonaceous component or the cosmic carbon abundance is overestimated), $x(H)$ is in the range 0.19–0.42. These constraints are shown as bold lines in the ternary phase diagram in Fig. 3 (left panel). The lower limit is the more stringent, as any other component of the ISM that consumes carbon (such as the gas phase CO) would decrease the available carbon abundance and thus increase the upper limit on the hydrogen content.

Placing this hydrogenated carbonaceous component of the DISM and the above-mentioned numerical limits into the context of a Random Covalent Network (RCN) yields further information (Phillips 1979; Dohler et al. 1980). RCN modeling states that the sum of the constraints applied to the constitutive elements of such a network is equal to the number of degrees of freedom. This leads to the equation

$$\sum_i x(i)N(i) = 3$$

where $x(i)$ is the atomic fraction of a network element (atom or cluster) involved and N_i the number of constraints per site occupied ($N(i) = m^2/2$ for $m \leq 2$ and $N(i) = 5m/2-3$ for $m \geq 2$, with m the coordination number). Many RCN models can be developed (e.g. Dadswell & Duley 1997) on this basis by adding the conservancy rule $x(H) + x(C_{sp^2}) + x(C_{sp^3}) = 1$. We focus on two kinds of networks which describe the two limiting cases for the C = C bonding type, either fully ethylenic (C2, model A) or fully aromatic (C6, model B). Model A leads to the following constraint (Angus & Jansen 1988):

$$0.5x(H) + 3.5x(C_{sp^2}) + 7x(C_{sp^3}) = 3$$

whereas the model B leads to the following constraint (Jones 1990):

$$0.5x(H) + 2x(C_{sp^2}) + 7x(C_{sp^3}) = 3.$$

These additional constraints are shown in the left panel of Fig. 3. The filled region around the hydrogen pole delineates where no network can be built because the hydrogen content is too high; only small molecules belong to this portion of the diagram. This is an additional constraint in the phase diagram.

In the right panel of Fig. 3 are plotted the positions or regions in which exist several laboratory-produced carbonaceous networks (Ferrari & Robertson 2000) involving diamond-like carbon, polymers or molecules. The position of our solution, the shaded area in the left hand phase diagram, from the RCN equation and astronomical constraints is in excellent agreement with the laboratory spectrum of a highly hydrogenated amorphous carbon, with the possibility of ethylenic/small aromatic structures linked by aliphatic bridges, but possessing few aromatic hydrogen terminations. This is radically different than the highly aromatic features observed in emission in other lines of sight, such as H II regions, where the relative abundance of aliphatic and aromatic materials is reversed.

The significant fraction of carbon in the sp^3 bonding state, observed in the DISM of IRAS 08572+3915, is consistent with the observed absence of carbon in aromatic form. If 15% of the total available carbon atoms along the line of sight are in sp^3 $CH_{n=2,3}$ bonds, then the carbonaceous network can develop few aromatic rings, as they require at least six carbon atoms each.

5. Conclusion

The extragalactic source IRAS 08572+3915 is an extreme case in which the 3–7 μm carbonaceous absorption bands in the DISM can be observed with a high optical depth and good sensitivity. That and a favorable redshift make this galaxy an optimal target for constraining the spectroscopic behavior of carbonaceous matter. The high column density of sp^3 bonds indicates that carbon in sp^3 bonds makes up the dominant fraction of the solid carbonaceous matter along the line of sight. By comparing the observed absorption features with a spectrum of laboratory-produced hydrogenated amorphous carbon we have shown that the observed dust is poor in hydrogenated aromatic structures, with a ratio of $H_{sp2}/H_{sp3} < 0.08$. Using a ternary phase diagram of candidate interstellar carbonaceous analogs, observed constraints and a random covalent network model we identify the observed interstellar hydrocarbons as belonging to the class of polymeric-like hydrogenated amorphous carbons, dominated by an aliphatic/olefinic backbone structure. Energetic processing of this material, in environments such as photodissociation regions, would selectively dehydrogenate the HAC, providing an opportunity for aromatic molecules to form. Thus, the carbonaceous material observed toward IRAS 08572+3915, and presumably also in the DISM toward the Galactic center, is probably the stable precursor to the aromatic infrared emission carriers in more energetic interface regions.

References

Angus, J. C., & Jansen, F. 1988, J. Vac. Sci. Technol. A, 6, 1778
Butchart, I., McFadzean, A. D., Whittet, D. C. B., Geballe, T. R., & Greenberg, J. M. 1986, A&A, 154, L5
Chiar, J. E., Pendleton, Y. J., Geballe, T. R., & Tielens, A. G. G. M. 1998, ApJ, 507, 281
Chiar, J. E., Adamson, A. J., Pendleton, Y. J., et al. 2002, ApJ, 570, 198
Dadswell, G., & Duley, W. W. 1997, ApJ, 476, 184
Dartois, E., Marco, O., Muñoz-Caro, G. M., et al. 2004a, A&A, 423, 549
Dartois, E., Muñoz Caro, G. M., Deboffle, D., & d'Hendecourt, L. 2004b, A&A, 423, L33
Dartois, E., Muñoz Caro, G. M., Deboffle, D., Montagnac, G., & D'Hendecourt, L. 2005, A&A, 432, 895
Dohler, G. H., Dandaloff, A. & Bilz, H. 1980, J. Noncrystalline Solids, 42, 87
Duley, W. W. 2000, ApJ, 528, 841
Duley, W. W., & Williams, D. A. 1983, MNRAS, 205, 67P
Duley, W. W., Scott, A. D., Seahra, S., & Dadswell, G. 1998, ApJ, 503, L183
Ehrenfreund, P., Robert, F., D'Hendencourt, L., & Behar, F. 1991, A&A, 252, 712
Evans, A. S., Mazzarella, J. M., Surace, J. A., & Sanders, D. B. 2002, ApJ, 580, 749
Ferrari, A. C., & Robertson, J. 2000, Phys. Rev., B 61, 14095
Geballe, T. R., Goto, M., Usuda, T., Oka, T., & McCall, B. J. 2006, ApJ, 644, 907
Geballe, T. R., Chiar, J., Pendleton, Y. J., & Tielens, A. G. G. M. 1997, Ap&SS, 255, 457
Hagen, W., Tielens, A. G. G. M., & Greenberg, J. M. 1983, A&AS, 51, 389
Dhendecourt, L. B., & Allamandola, L. J. 1986, A&AS, 64, 453
Houck, J. R., et al. 2004, ApJS, 154, 18
Hudgins, D. M., & Sandford, S. A. 1998a, J. Phys. Chem., 102, 329
Imanishi, M. 2000, MNRAS, 319, 331
Imanishi, M., Dudley, C. C., & Maloney, P. R. 2006, ApJ, 637, 114
Joblin, C., D'Hendecourt, L., Leger, A., & Defourneau, D. 1994, A&A, 281, 923
Jones, A. P. 1990, MNRAS, 247, 305
Jones, T. J., Hyland, A. R., & Allen, D. A. 1983, MNRAS, 205, 187
Leger, A., D'Hendecourt, L., & Defourneau, D. 1989, A&A, 216, 148
Mason, R. E., Wright, G., Pendleton, Y., & Adamson, A. 2004, ApJ, 613, 770
McFadzean, A. D., Whittet, D. C. B., Bode, M. F., Adamson, A. J., & Longmore, A. J. 1989, MNRAS, 241, 873
Mennella, V., Brucato, J. R., Colangeli, L., & Palumbo, P. 2002, ApJ, 569, 531
Moore, M. H., & Donn, B. 1982, ApJ, 257, L47
Mountain, C. M., Robertson, D. J., Lee, T. J., & Wade, R. 1990, Proc. SPIE, 1235, 25
Pendleton, Y. J., & Allamandola, L. J. 2002, ApJS, 138, 75
Phillips, J. C. 1979, Phys. Rev. Lett., 42, 1151
Rieke, G. H., & Lebofsky, M. J. 1985, ApJ, 288, 618
Roche, P. F., & Aitken, D. K. 1984, MNRAS, 208, 481
Sandford, S. A., Allamandola, L. J., Tielens, A. G. G. M., Sellgren, K., Tapia, M., & Pendleton, Y. 1991, ApJ, 371, 607
Sandford, S. A., Pendleton, Y. J., & Allamandola, L. J. 1995, ApJ, 440, 697
Schutte, W. A., Tielens, A. G. G. M., Allamandola, L. J., Wooden, D. H., & Cohen, M. 1990, ApJ, 360, 577
Spoon, H. W. W., Keane, J. V., Tielens, A. G. G. M., et al. 2002, A&A, 385, 1022
Spoon, H. W. W., Armus, L., Cami, J., et al. 2004, ApJS, 154, 184
Spoon, H. W. W., Tielens, A. G. G. M., Armus, L., et al. 2006, ApJ, 638, 759
Tielens, A. G. G. M., Wooden, D. H., Allamandola, L. J., Bregman, J., & Witteborn, F. C. 1996, ApJ, 461, 210
Werner, M. W., et al. 2004, ApJS, 154, 1
Wexler, A. S. 1965, Spectrochim. Acta, 21(10), 1725
Wexler, A. S. 1967, Appl. Spec. Rev., 1, 29
Wright, G. S., Bridger, A., Geballe, T. R., & Pendleton, T. 1996, in New Extragalactic Perspectives in the New South Africa, ed. D. L. Block, & J. M. Greenberg (Dordrecht: Kluwer), 143